

Bayesian Deep Networks for Supervised Single-View Depth Learning

Javier Rodríguez-Puigvert, Rubén Martínez-Cantín, Javier Civera

Abstract—Uncertainty quantification is a key aspect in robotic perception, as overconfident or point estimators can lead to collisions and damages to the environment and the robot. In this paper, we evaluate scalable approaches to uncertainty quantification in single-view supervised depth learning, specifically MC dropout and deep ensembles. For MC dropout, in particular, we explore the effect of the dropout at different levels in the architecture. We demonstrate that adding dropout in the encoder leads to better results than adding it in the decoder, the latest being the usual approach in the literature for similar problems. We also propose the use of depth uncertainty in the application of pseudo-RGBD ICP and demonstrate its potential for improving the accuracy in such a task.

I. INTRODUCTION

The quantification of the uncertainty in the fields of robotics and computer vision is critical to develop more robust and reliable systems. Point estimators, which dominate among others the landscape of multi-view [20], [5] and single-view [7], [10] structure estimation, do not usually estimate uncertainties. Higher-level decision blocks using them have no means, then, to judge how confident they are and cannot use such information for task planning. Uncertainty is often present in the formulation of model-based estimators (e.g., [1]), but it is scarce in learning-based approaches. Furthermore, learning-based approaches tend to overfit on standard datasets, which might lead us to assume a reasonable general performance while they are strongly biased. In such cases, their outputs should not be trusted in real-world applications, for which we would need generalizable and self-aware models. The use of Bayesian learning is one of the approaches that will alleviate such problems.

In this work, we evaluate the two different sources of uncertainty –epistemic and aleatoric– in single-view depth learning with the aim to determine the quality of the model predictions and hence its potential for robotic applications. In neural networks, uncertainty can stem from the input data or the network weights. For the latter, scalable approaches to Bayesian deep learning have shown to be effective to model uncertainty. Fig. 1 shows the output of our Bayesian framework for supervised single-view depth learning. Notice first the small depth error, but most importantly, how such error is mostly coherent with the predicted uncertainty. Finally, see that in this case, the aleatoric uncertainty is in general bigger, but the epistemic uncertainty is still relevant and necessary. In some other examples, we will show that the epistemic uncertainty can be even bigger.

The authors are with I3A, Universidad de Zaragoza, Spain.
 {jrp, rmcantin, jcivera}@unizar.es

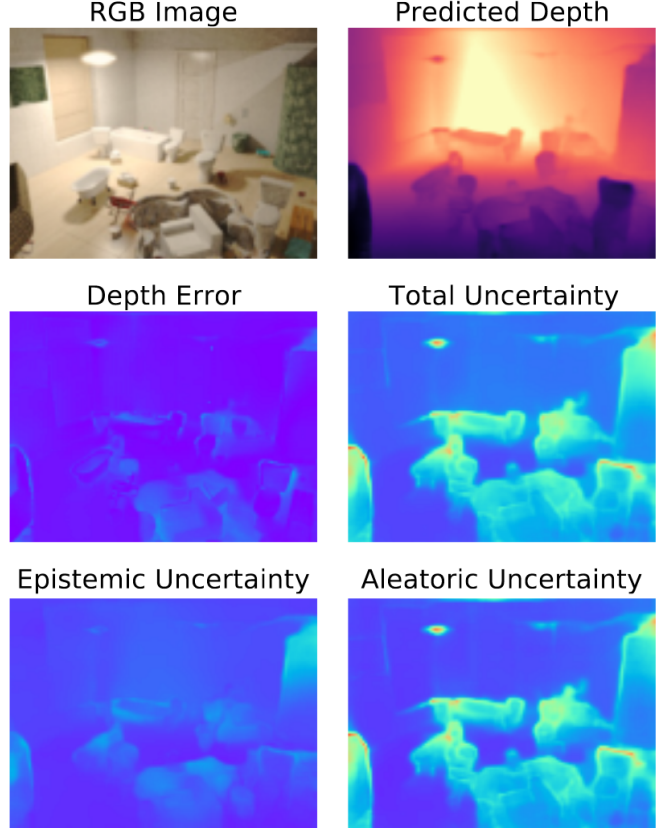


Fig. 1: Bayesian single-view depth estimation in a SceneNet image. Notice in the middle row the accuracy of the depth error, and how the predicted total uncertainty matches it. Notice also in the bottom row how both epistemic and aleatoric uncertainty are both significant and relevant for a correct uncertainty quantification.

The contributions of this work are: first, we provide a unified framework and a thorough evaluation of scalable uncertainty estimation approaches, namely Monte Carlo (MC) dropout and deep ensembles, for supervised single-view depth learning with deep networks. Secondly, we propose to apply MC dropout in the encoder, contrary to recent works [11], [22] that apply it in the decoder for similar tasks. We demonstrate in our evaluations that, in our particular task of supervised depth learning, the dropout in the encoder achieves a better performance than the dropout in the decoder. Such a result has relevant practical implications, as MC dropout has a lower memory footprint than ensembles. Finally, we also provide initial results in pseudo-RGBD ICP, a potential application for our single-view depth uncertainty

models. With such final experiments, we demonstrate that our uncertainty estimates are reasonably well calibrated and already offer promising improvements, but also that further research is still needed for a full integration in probabilistic approaches.

II. BACKGROUND AND RELATED WORK

A. Structure Estimation and Learning from Images

Understanding the 3D structure of a scene from visual data is a key prerequisite for many relevant applications, such as augmented reality or robotics. This task has been addressed from a wide variety of perspectives, being the more mature ones based on multiple images either alone [20], [5] or fused with other sensors (e.g., visual-inertial approaches [23]).

However, such multi-view and visual-inertial pipelines present two main limitations: they require sufficiently textured scenes to find correspondences between images, and also need sufficient sensor motion. Single-view depth learning can potentially overcome these two issues, although it is significantly more challenging due to its ill-posed nature.

Following the seminal work on learning-based depth estimation [26], Eigen et al. [4] was the first one using deep networks with supervised training, specifically a scale-invariant loss and a coarse to fine architecture. Many works have followed with different contributions: Laina et al. [15] proposed deeper fully convolutional models with impressive results. Fu et al. [7] proposed a spacing-increasing depth discretization that learns depth from an ordinal regression perspective. Dijk and de Croon [3] evaluated a self-trained single-view depth network to investigate on which visual cues the network is relying. From their conclusions, depth networks favor vertical positions and disregard obstacles in their apparent size. Similarly, our work contributes to understanding the behavior of depth networks from a Bayesian perspective.

Several works have proposed self-supervised approaches, using photometric reprojection losses between stereo or multiple views [9], [30]. However, self-supervised approaches still underperform compared to supervised ones. For this reason, and given the current abundance of RGB-D data and the huge growth and potential of such sensors, we focus on supervised methods.

B. Bayesian Deep Learning

Bayesian deep learning combines the strengths and flexibility of deep learning methods with the uncertainty quantification of probabilistic (Bayesian) learning and inference methods. For uncertainty quantification, we must identify what the model does not know versus what is missing from the data. Therefore, the uncertainty sources can be classified into two: aleatoric and epistemic. Aleatoric uncertainty, sometimes referred to as statistical uncertainty, refers to the uncertainty caused by the realization of different experiments. In machine learning, it encodes the variability in the different inputs from the dataset. Thus, this type of uncertainty cannot be reduced by increasing the amount of training data. Most models assume that the aleatoric

uncertainty is also homoscedastic; that is, it is independent of the input data. In this work, we train the network to predict the uncertainty for each input datum resulting in a heteroscedastic uncertainty model [14], [2].

Epistemic uncertainty, also known as systematic uncertainty, represents the lack of knowledge of our trained model. This type of uncertainty is deeply related to the training data and the model ability to generalize. For example, epistemic uncertainty is high when the network faces out-of-distribution data or has to extrapolate in areas where training data was scarce. In Bayesian deep learning, the epistemic uncertainty can be estimated from the uncertainty in the model parameters, assuming that the model architecture is correct. In this case, epistemic uncertainty can be obtained using a prior distribution $p(\theta)$ over the neural network parameters θ and computing its posterior distribution $p(\theta|\mathcal{D})$ given a dataset \mathcal{D} using Bayes rule: $p(\theta|\mathcal{D}) = \frac{p(\mathcal{D}|\theta)p(\theta)}{p(\mathcal{D})}$. In general, this equation is intractable in Bayesian deep learning, but there are several approaches to tackle this problem that we describe below.

Variational inference (VI). VI proposes the use of a tractable approximation $q(\theta)$ to the posterior distribution $p(\theta|\mathcal{D})$. Mean-field variational inference assumes an isotropic Gaussian distribution for $q(\theta) \sim \mathcal{N}(\theta|\mu, \mathbf{I}\sigma)$. The parameters of the approximate distribution $q(\theta)$ are optimized by minimizing the KL-divergence between the approximate distribution and the true posterior $D(q||p)$. Mean-field variational inference with Gaussian approximation suffers from the soap-bubble effect, reducing the predictive performance as most samples fall in a ring. The Radial Bayesian Neural Networks [6] avoid that effect, but the distribution is biased towards the center resulting in uncertainty underestimation. Furthermore, VI methods are very sensitive to calibration and configuration. A natural-gradient VI method [21] was introduced to improve the robustness of the optimization. However, it requires strong approximations of the Hessian, resulting in lower performance.

Monte Carlo (MC) Dropout. MC dropout can be used to approximate the posterior distribution, as proposed in [8]. It can be considered as a specific case of VI, where the variational distribution includes a set of binary random variables that represent the corresponding unit to be turned off or dropped. The approximation makes the computation more tractable and robust. MC dropout is able to approximate multimodal distributions. However, the epistemic distribution on the weight-space only has discrete support. Kendall and Gal [14] presented a framework to combine both aleatoric and epistemic uncertainty, where MC dropout is used to obtain epistemic uncertainty, while the function mapping the aleatoric uncertainty is learned by a map function of the input data.

Deep Ensembles. Deep ensembles [16] involves training the same architecture many times optimizing some MAP loss, but starting from different random initialization of its parameters. Therefore, deep ensembles are not truly a Bayesian approach as the samples are distributed according to the different local optima. Conversely, these models in

an ensemble perform reasonably well, even considering the small number of random samples considered in practice, as all of the models are optimized and have a high likelihood. Therefore, deep ensembles can be considered an approximate Bayesian model average, although, in practice, they can also be used as a rough posterior approximation. Contrary to MC dropout, where the model weights are shared between samples, in the case of deep ensembles, each *sample* is trained independently. Therefore the number of model parameters required grows linearly with the number of samples. Furthermore, deep ensembles also result in a distribution with discrete support on the weight-space.

C. Bayesian Deep Learning in Computer Vision

Evaluating uncertainty correctly is still in open discussion, as it is task-related. Mukhoti and Yal [19] evaluated MC dropout in semantic segmentation networks. They designed metrics for the segmentation task to provide benchmarks for future comparison. Similarly, Gustafsson et al. [11] designed a framework to explore uncertainty metrics for semantic segmentation and depth completion, using MC dropout and deep ensembles. In the context of single-view depth, Poggi et al. [22] evaluated the uncertainty of self-supervised networks, using the photo-metric error in their loss to regress depth. They observed that the depth accuracy is improved by uncertainty estimation along the training paradigms. Our work complements this evaluation with a related evaluation of the supervised setting.

III. BAYESIAN SINGLE-VIEW DEPTH LEARNING FROM SUPERVISED DATA

As seen in section II-B, both MC dropout and deep ensembles provide a sample representation of the posterior distribution over the network parameters. In this work, we introduce a unified formulation to analyze the posterior and predictive distribution for these sample representations. For brevity, we have expressed the framework for our application of depth perception, although the framework can be extended to other problems of Bayesian deep learning.

A. Architecture and Loss

For single-view depth estimation, we adapt the encoder-decoder architecture of [10], inspired by the work of [24]. The encoder is a Resnet18 [12] initialised with pre-trained weights from imageNet [25]. The architecture of the decoder is summarized in Table I.

The network is trained with a dataset $\mathcal{D} = \{\{\mathcal{I}_1, d_1\}, \dots, \{\mathcal{I}_N, d_N\}\}$, composed by N supervised pairs, each pair $i \in \{1, \dots, N\}$ containing the input image $\mathcal{I}_i \in \{0, \dots, 255\}^{w \times h \times 3}$ and its ground truth depth $d_i \in \mathbb{R}_{>0}^{w \times h}$ and network weights θ . For a single input image, the network $f_\theta(\mathcal{I})$ outputs two channels: the depth estimation $\hat{d}(\mathcal{I})$ and the depth uncertainty $\sigma_d^2(\mathcal{I})$, both per pixel. The later corresponds to the aleatoric uncertainty, which can also be interpreted as heteroscedastic observation noise. We incorporate both output channels in a single loss per image by using a standard Gaussian log-likelihood [14]:

Depth Decoder			
layer	# filters	inputs	activation
upconv5	256	econv5	ELU
iconv5	256	\uparrow upconv5, econv4	ELU
upconv4	128	iconv5	ELU
iconv4	128	\uparrow upconv4, econv3	ELU
depth_unc4	2	iconv4	-
upconv3	64	iconv4	ELU
iconv3	64	\uparrow upconv4, econv3	ELU
depth_unc3	2	iconv3	-
upconv2	32	iconv3	ELU
iconv2	32	\uparrow upconv2, econv1	ELU
depth_unc2	2	iconv2	-
upconv1	16	iconv2	ELU
iconv1	16	\uparrow upconv1	ELU
depth_unc1	2	iconv1	-

TABLE I: Decoder architecture. Kernels are 3×3 and stride 1 for all convolutions. \uparrow stands for 2×2 nearest-neighbor upsampling.

$$\mathcal{L}(\theta) = \frac{1}{w \cdot h} \sum_{j \in \mathcal{I}} \frac{\|d_j - \hat{d}(\mathcal{I}_j)\|^2}{2\sigma_d^2(\mathcal{I}_j)} + \frac{1}{2} \log \sigma_d^2(\mathcal{I}_j) \quad (1)$$

where $j \in \mathcal{I}$ is the pixel index of the image of size $w \cdot h$.

For deep ensembles, the loss function is evaluated independently for each sample model because they are trained separately, resulting in a set of $\{\theta_m\}_{m=0}^M$ different parameters, one for each sample model. Although the sample models are not drawn from the posterior distribution, the latter can be considered an approximation in practice. Deep ensembles are especially suitable for our problem as we need to maintain the number of samples small to keep it tractable. Therefore, it is important that we are not wasting valuable resources in low probability models that might reduce the overall performance.

In the case of MC dropout, the loss function can be used to perform approximate variational inference on the posterior distribution on the model weights by training on that loss function with dropout before every weight layer. The actual Monte Carlo phase is done by also performing random dropout at test time to sample from the variational distribution computed during training [14]. This sampling at test time results again in a set of $\{\theta_m\}_{m=0}^M$ different parameters. Note that this time, they are all generated from the same trained model, resulting in a much lower memory and computational footprint compared to deep ensembles or other variational methods. In practice, we found that adding dropout at every layer reduced the predictive performance considerably for our application, which is consistent with previous results [19]. Therefore, in section IV-C, we study different configurations of dropout and compare both the quality in terms of predictions and uncertainty quantification.

B. Bayesian prediction of sample-based deep networks

The predictive distribution for a pixel depth can be computed by integrating over the model parameters. We can use the same strategy for both MC dropout and deep ensembles as they are both use sample representations of the model

parameters:

$$\begin{aligned} p(d|\mathcal{I}, \mathcal{D}) &= \int p(d|\mathcal{I}, \theta)p(\theta|\mathcal{D})d\theta \\ &\approx \sum_{m=0}^M p(d|\mathcal{I}, \theta_m) \end{aligned} \quad (2)$$

Because our architecture generates a Gaussian prediction for the pixel depth $\mathcal{N}(\hat{d}, \sigma_d^2)$, the sample-based output is a mixture of Gaussians that can be approximated by a single Gaussian. In particular, for the $\{\theta_m\}_{m=0}^M$ model samples (MC Dropout) or models (ensembles) with respective outputs $\hat{d}(m)$ and $\sigma_d^2(m)$, we approximate the total predictive distribution for each pixel as a Gaussian distribution $p(d|\mathcal{I}, \mathcal{D}) \approx \mathcal{N}(\hat{d}_t, \sigma_t^2)$ with:

$$\begin{aligned} \hat{d}_t &= \frac{1}{M} \sum_{m=0}^M \hat{d}_m \\ \sigma_t^2 &= \underbrace{\frac{1}{M} \sum_{m=0}^M \left(\hat{d}_t - \hat{d}(m) \right)^2}_{\text{epistemic}} + \underbrace{\frac{1}{M} \sum_{m=0}^M \sigma_d^2(m)}_{\text{aleatoric}} \end{aligned} \quad (3)$$

In the experiments, we will show that identifying and quantifying the epistemic from the aleatoric uncertainty will be fundamental to finding the uncertainty source and improving the quality of the model and the predictions.

IV. EXPERIMENTS

A. Dataset

For our experiments, we use the SceneNet RGB-D dataset [18], containing photorealistic sequences of synthetic indoor scenes from very general camera trajectories, along with their ground truth. Our models are trained over 210,000 synthetic images of 700 scenes and tested on 90,000 images of 300 different scenes. We chose this dataset as it provides a wide variety of viewpoints and scenes, challenging occlusions and different lighting conditions, which are relevant for the network generalization. The availability of ground truth is also relevant for a solid evaluation of the errors.

B. Metrics

We evaluate the depth errors of the different models by using the metrics that are standard in literature: Absolute Relative difference, Square Relative difference, RSME, RMSE log and $\delta < 1.25^i$ with $i \in \{1, 2, 3\}$ (see their definitions in [4]). For the pseudo-RGBD Bayesian ICP, we report the translational and rotational RSME.

While the above error metrics are well established in literature, uncertainty-related ones are more task-dependent. In our evaluation, we use pixel-wise uncertainty metrics, specifically the Area Under the Calibration Error curve (AUCE) and Area Under the Sparsification Error curve (AUSE). Following the procedure in Gustafsson et al. [11], we define 100 prediction intervals of confidence level $p \in [0, 1]$ and use the cumulative density function of our output distribution (Gaussian). For each confidence level, we expect for a perfect calibration that the ratio of the prediction

interval covering the true target \hat{p} to be identical to the confidence level p . AUCE is defined as the area between the absolute error curve with respect to a perfect calibration $|p - \hat{p}|$. AUSE is used to measure the uncertainty calibration. Introduced by Ilg et al. [13], it is a relative measure of uncertainty. This metric compares the ordering of the per-pixel uncertainties against the order of the per-pixel depth errors. The ordering should be similar for a well-calibrated uncertainty, as uncertain predictions will tend to have larger errors.

C. Bayesian Single-View Depth

We evaluate several variations of MC dropout and deep ensembles, specifically:

MC Dropout. For MC dropout, we explore the depth and uncertainty outcomes for dropouts at different levels of the chosen architecture, and also for different numbers of forward passes. For each setting we train two models with $p = 0.3$ and $p = 0.5$, p being the probability of an element to be zeroed. Regarding the specific layers where dropout is applied, we evaluate two specific configurations.

MC Dropout Decoder. We apply dropout only in the decoder and examine whether this affects the recomposition of the feature maps obtaining epistemic uncertainty for deterministic encoding. The dropout layer is introduced after the last four convolutional layers of the encoder.

MC Dropout Encoder. Dropout is applied in the encoder to see how it influences the encoding of the feature maps leading to a variance throughout the whole network. Inspired by Mukhoti and Gal [19], we place the dropout after the last convolutional layer of the encoder and after every convolutional layer in the decoder.

Deep Ensembles. We examine uncertainty and depth by averaging an ensemble composed of a variable number of networks (up to 18). We initialise the network weights with different seeds from a normal distribution $\mathcal{N}(0, 10^{-3})$.

Results. Table II presents the performance metrics for the depth and its uncertainty for relevant variations of MC dropout and deep ensembles. In our experiments, MC dropout outperforms, in general, the deep ensembles.

The MC dropout models themselves show a significant variation in their performance. We found that introducing dropout in the encoder (models named as MC Dropout Encoder) leads to lower errors than introducing it in the decoder (models named as MC Dropout Decoder). This result is relevant, as MC Dropout in the decoder is the usual practice [11], [22]. Intuitively, we believe that applying MC dropout in the decoder produces deterministic image representations because the encoder is deterministic. In contrast, MC dropout in the image encoder allows us to have probabilistic representations and consider uncertainty in the feature space, which seem a more appropriate model for Bayesian image processing. Looking at the different dropout parameters, the depth prediction improves if we lower the influence of dropout in the network from 0.5 to 0.3.

Our results are summarized in Fig. 2. In this figure, it can be appreciated how depth errors are reduced and

Model	M	Abs Rel	Sq Rel	RMSE	RMSE Log	$\delta < 1.25$	$\delta < 1.25^2$	$\delta < 1.25^3$	AUCE	AUSE
MC Dropout Decoder 0.3	16	0.17860	0.27275	0.72885	0.25977	0.83910	0.95325	0.97946	0.48512	0.16107
MC Dropout Decoder 0.3	32	0.17766	0.27128	0.72602	0.25888	0.84066	0.95369	0.97961	0.48485	0.16055
MC Dropout Decoder 0.5	16	0.19495	0.29254	0.76940	0.27299	0.82018	0.94699	0.97643	0.48657	0.16205
MC Dropout Decoder 0.5	32	0.19305	0.28910	0.76289	0.115	0.82331	0.94801	0.97683	0.48615	0.16082
MC Dropout Encoder 0.5	16	0.1571	0.2221	0.6858	0.2404	0.8559	0.9574	0.9815	0.48411	0.14633
MC Dropout Encoder 0.5	32	0.1568	0.2212	0.6843	0.2399	0.8564	0.9576	0.9816	0.4840	0.14485
MC Dropout Encoder 0.3	16	0.1494	0.20562	0.6780	0.2363	0.8604	0.9596	0.9825	0.48456	0.14500
MC Dropout Encoder 0.3	32	0.1491	0.2050	0.6770	0.2359	0.8608	0.9598	0.9826	0.4845	0.1436
Deep Ensembles	14	0.2077	0.2912	0.8805	0.2880	0.7478	0.9200	0.9709	0.48469	0.14305
Deep Ensembles	18	0.2072	0.2904	0.8784	0.2876	0.7486	0.9203	0.9709	0.4846	0.1426

TABLE II: Depth and uncertainty metrics for several variations of MC Dropout and Deep Ensembles in SceneNet RGB-Depth. Best results are boldfaced.

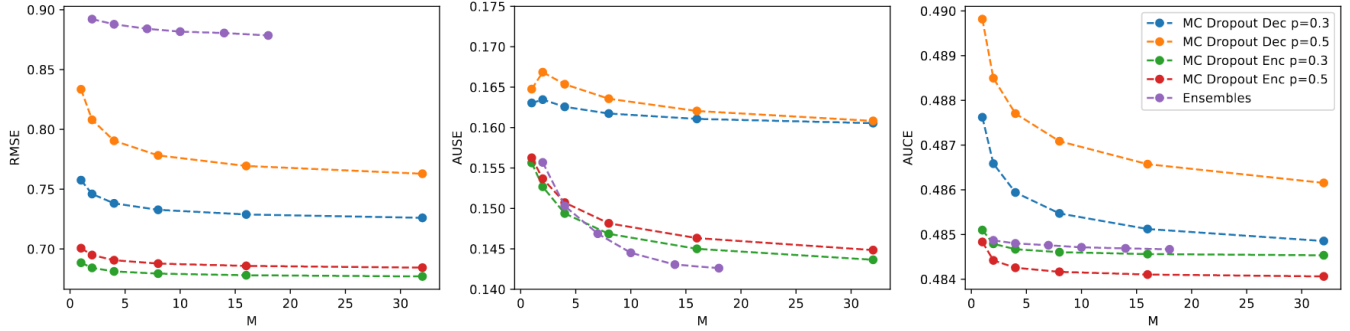


Fig. 2: Comparison of MC Dropout Decoder 0.3, Decoder 0.5, Encoder 0.3, Encoder 0.5, and Deep Ensembles for different numbers of forward passes M . Left: RMSE. Center: AUSE. Right: AUCE. The higher M is, the better the performance, but with slight improvements for $M > 18$. Overall, the models MC Dropout Encoder offer the best metrics.

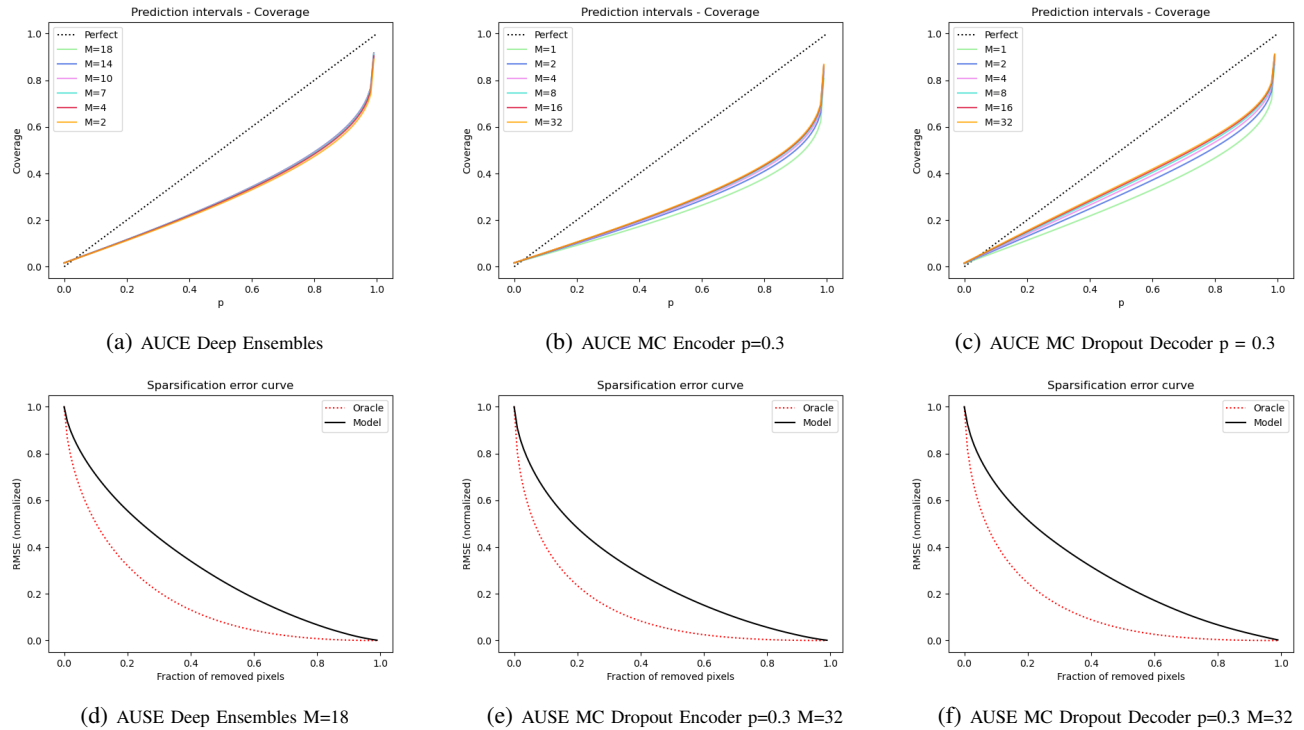


Fig. 3: Calibration plots for MC Dropout and Deep Ensembles. Calibration Error Curve and Sparsification Error Curve.

then uncertainty representation improve with the number of forward passes M , both for MC dropout and ensembles. However, there is a diminishing return with higher values

of M , being the improvement very small for $M > 18$.

Regarding the uncertainty quantification, we observe that the epistemic uncertainty is high for data on the margins

of the distribution and is clear to see when the image contains mirrors or surfaces with little or no texture. Aleatoric uncertainty appears mainly in depth discontinuities, at the edges of objects, and regions with sharp contrast in lighting (see Fig. 4). As additional qualitative examples to further understand the performance of our approach, Fig. 5 shows highly uncertain depth predictions for two out-of-distribution images. It indicates high uncertainty values for unfamiliar objects not seen during training, like the dog and the door in the background in the first picture, as well as for the unrealistic patterns of the painting “Bedroom in Arles” by Van Gogh.

The AUSE values (Fig. 2 and Fig. 3) demonstrate that the uncertainty model is better calibrated with deep ensembles. In its best configuration, deep ensembles outperform slightly MC dropout encoder 0.5 and MC dropout encoder 0.3. Nevertheless, looking at the AUCE values representing the coverage of prediction intervals, we observe that MC dropout encoder 0.5 is the best model. The difference in the uncertainty metrics is small for all the models, but we can observe that MC dropout in the decoder performs consistently worse than the rest. It should be remarked that the metrics are still far from the perfect value of 0, suggesting that further research is needed on improving uncertainty models.

Finally, Fig. 3 show the calibration error curves and sparsification error curves from where AUSE and AUCE were extracted, for some of our models. In this figures it can be seen that all models have overconfident uncertainties, and the similarity between the sparsification error curves that leads to similar AUSE values.

D. Bayesian Pseudo-RGBD ICP

We evaluate the application of Bayesian depth networks to estimate the relative motion between two monocular images. When it comes to estimating the motion from two monocular views, geometric methods commonly outperform learning-based methods [29]. However, geometric methods for two monocular views have two limitations: first, the scale factor cannot be recovered. And second, finding correspondences might be challenging in weakly textured scenes.

Our proposal is leveraging the depth predicted by a network to augment monocular images into what we call pseudo-RGBD views and then aligning the point clouds using ICP. Similar ideas were proposed recently in [28], [17]. Differently from us, they rely on Structure from Motion [27] or visual SLAM [20] to estimate the motion from the pseudo-RGBD views. Also, we use our depth uncertainty for a more informed point cloud alignment, specifically excluding highly uncertain points in the ICP.

Percentile	.30	.50	.75	.90	.95	.99	1.00
# best t	625	607	599	444	362	286	431
RMSE t [m]	0.565	0.430	0.347	0.327	0.335	0.342	0.342
# best r	452	565	643	474	359	321	540
RMSE r [°]	12.602	9.568	7.162	6.646	6.303	6.245	6.360

TABLE III: Evaluation of ICP for percentiles .30, .50, .75, .90, .95, .99, 1.00. Best are boldfaced.

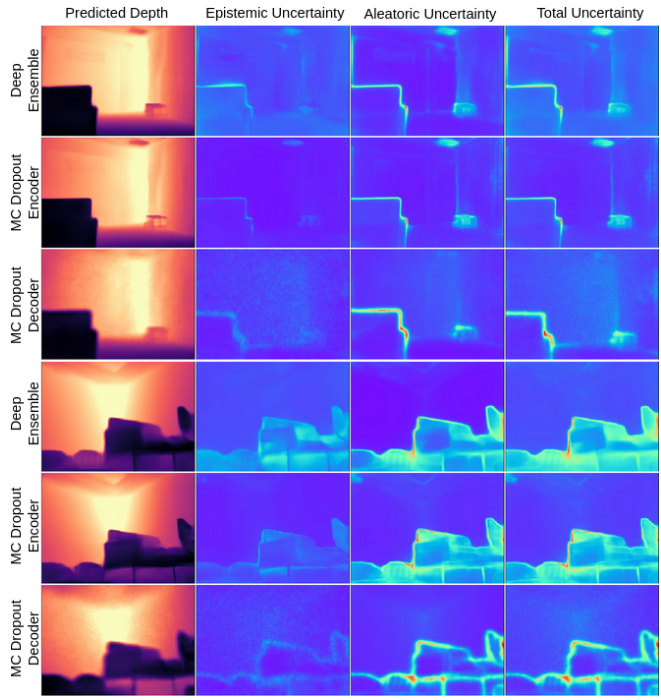


Fig. 4: Qualitative results for depth and uncertainty in two frames of scene 374 of SceneNet RGB-D, showing aleatoric uncertainty mostly in depth discontinuities and epistemic uncertainty in regions with low texture.

Our experimental setup is as follows. We selected 3,354 random image pairs from the SceneNet RGB-D dataset, for which their separation is 4 frames. We excluded pairs for which there were large areas without ground-truth depth (e.g., windows) and rotations were larger than 30° (ICP does not converge easily from distant initial seeds). For each pair, we back-projected the RGB-D views and the depth uncertainty into point clouds, and we compute ICP using the following percentiles of the most certain points according to our uncertainty estimation: .30, .50, .75, .90, .95, .99 and 1.00 (the percentile 1.00 corresponds to the full point clouds). We used our model MC Dropout Encoder 0.3, as it was the best performing in Table II.

Fig. 6 illustrates our aim with an example. The left point cloud is the original one, and the right one corresponds to the percentile .90, with the 10% most uncertain points that were left out colored in red. Notice how the most uncertain points correspond with the ones with the highest errors, located mainly on depth discontinuities. Removing such highly erroneous points from ICP will, in principle, improve its accuracy.

Table III aggregates the quantitative evaluation for all our image pairs. As the first metric (# **best t**), we report the number of times each percentile shows the best accuracy in translation. The percentile .30, for which 70% of the points with the highest uncertainty were removed, performs best in this metric. Notice that, for the number of times each percentile is best in rotational RMSE (# **best t**), the percentile .75 shows the best result. In both of the cases removing

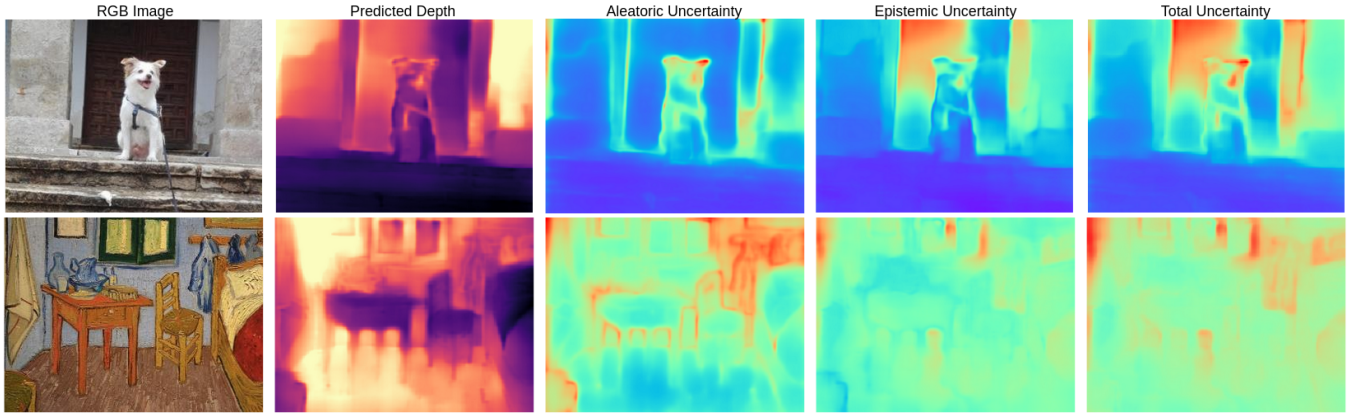


Fig. 5: Depth and uncertainty for two out-of-distribution images, showing high uncertainty values for unfamiliar objects and textures. Top row: We can see that both uncertainties capture different sources. The aleatoric uncertainty is large in depth discontinuities and at the edge of objects, and the epistemic uncertainty is large in the unknown regions or surfaces with little or no texture. Bottom row: the aleatoric and epistemic uncertainties are both large due to the large differences in appearance with respect to the training data.



Fig. 6: Left: Point cloud produced by our depth network. Right: Same point cloud, with the top 10% most uncertain points are plotted in red. These points corresponds to spurious or high error points that will degrade the performance of ICP.

highly uncertain points improves significantly over keeping the original point clouds (percentile 1.00). See also that, for the average rotational and translational RMSE (**RMSE r** and **RMSE t**), the best performers are .99 and .90, and keeping all the points ranks on third and fourth position respectively. These metrics evidence that the uncertainties estimated by our models are well-calibrated.

V. CONCLUSIONS

In this paper, we evaluated MC dropout and deep ensembles as scalable Bayesian approaches to uncertainty quantifi-

cation for single-view supervised depth learning. We have demonstrated that MC dropout in the encoder outperforms the current approach of using it in the decoder. In our experiments, depth estimation has a better representation when we use MC dropout on the encoder, but deep ensembles are the slightly better option to represent uncertainty. We also demonstrated the application of uncertainty to pseudo-RGBD ICP with the result that relative transformation can be improved by excluding the points with higher uncertainties. For future investigation into this topic, we need to address

the overconfidence that we observed in our depth prediction networks and research a better representation of uncertainty. Furthermore, it would be interesting to investigate how to benefit from the posterior computation to overcome the domain change in the case of real data.

REFERENCES

- [1] T. D. Barfoot. *State estimation for robotics*. Cambridge University Press, 2017.
- [2] A. Der Kiureghian and O. Ditlevsen. Aleatory or epistemic? does it matter? *Structural Safety*, 31:105–112, 03 2009.
- [3] T. v. Dijk and G. de Croon. How do neural networks see depth in single images? In *Proceedings of the IEEE/CVF International Conference on Computer Vision*, pages 2183–2191, 2019.
- [4] D. Eigen, C. Puhrsch, and R. Fergus. Depth map prediction from a single image using a multi-scale deep network. *arXiv preprint arXiv:1406.2283*, 2014.
- [5] J. Engel, V. Koltun, and D. Cremers. Direct sparse odometry. *IEEE transactions on pattern analysis and machine intelligence*, 40(3):611–625, 2017.
- [6] S. Farquhar, M. Osborne, and Y. Gal. Radial bayesian neural networks: Beyond discrete support in large-scale bayesian deep learning. *Proceedings of the 23rd International Conference on Artificial Intelligence and Statistics*, 2020.
- [7] H. Fu, M. Gong, C. Wang, K. Batmanghelich, and D. Tao. Deep ordinal regression network for monocular depth estimation. *Proceedings of the IEEE Computer Society Conference on Computer Vision and Pattern Recognition*, pages 2002–2011, 2018.
- [8] Y. Gal and Z. Ghahramani. Dropout as a bayesian approximation: Representing model uncertainty in deep learning. In *international conference on machine learning*, pages 1050–1059. PMLR, 2016.
- [9] C. Godard, O. Mac Aodha, and G. J. Brostow. Unsupervised monocular depth estimation with left-right consistency. *Proceedings - 30th IEEE Conference on Computer Vision and Pattern Recognition, CVPR 2017*, 2017-Janua:6602–6611, 2017.
- [10] C. Godard, O. Mac Aodha, M. Firman, and G. J. Brostow. Digging into self-supervised monocular depth estimation. In *Proceedings of the IEEE/CVF International Conference on Computer Vision*, pages 3828–3838, 2019.
- [11] F. K. Gustafsson, M. Danelljan, and T. B. Schon. Evaluating scalable bayesian deep learning methods for robust computer vision. In *Proceedings of the IEEE/CVF Conference on Computer Vision and Pattern Recognition Workshops*, pages 318–319, 2020.
- [12] K. He, X. Zhang, S. Ren, and J. Sun. Deep residual learning for image recognition. In *Proceedings of the IEEE conference on computer vision and pattern recognition*, pages 770–778, 2016.
- [13] E. Ilg, Ö. Çiçek, S. Gaësso, A. Klein, O. Makansi, F. Hutter, and T. Brox. Uncertainty estimates and multi-hypotheses networks for optical flow. *Lecture Notes in Computer Science (including subseries Lecture Notes in Artificial Intelligence and Lecture Notes in Bioinformatics)*, 11211 LNCS:677–693, 2018.
- [14] A. Kendall and Y. Gal. What uncertainties do we need in Bayesian deep learning for computer vision? *Advances in Neural Information Processing Systems*, 2017-Decem(Nips):5575–5585, 2017.
- [15] I. Laina, C. Rupprecht, V. Belagiannis, F. Tombari, and N. Navab. Deeper depth prediction with fully convolutional residual networks. In *2016 Fourth international conference on 3D vision (3DV)*, pages 239–248. IEEE, 2016.
- [16] B. Lakshminarayanan, A. Pritzel, and C. Blundell. Simple and scalable predictive uncertainty estimation using deep ensembles. *Advances in Neural Information Processing Systems*, 2017-December(Nips):6403–6414, 2017.
- [17] X. Luo, J.-B. Huang, R. Szeliski, K. Matzen, and J. Kopf. Consistent video depth estimation. *ACM Transactions on Graphics (TOG)*, 39(4):71–1, 2020.
- [18] J. McCormac, A. Handa, S. Leutenegger, and A. J. Davison. Scenenet rgb-d: 5m photorealistic images of synthetic indoor trajectories with ground truth. *arXiv preprint arXiv:1612.05079*, 2016.
- [19] J. Mukhoti and Y. Gal. Evaluating bayesian deep learning methods for semantic segmentation. *arXiv preprint arXiv:1811.12709*, 2018.
- [20] R. Mur-Artal and J. D. Tardós. Orb-slam2: An open-source slam system for monocular, stereo, and rgb-d cameras. *IEEE Transactions on Robotics*, 33(5):1255–1262, 2017.
- [21] K. Osawa, S. Swaroop, A. Jain, R. Eschenhagen, R. E. Turner, R. Yokota, and M. E. Khan. Practical deep learning with bayesian principles. *arXiv preprint arXiv:1906.02506*, 2019.
- [22] M. Poggio, F. Aleotti, F. Tosi, and S. Mattoccia. On the uncertainty of self-supervised monocular depth estimation. In *Proceedings of the IEEE/CVF Conference on Computer Vision and Pattern Recognition*, pages 3227–3237, 2020.
- [23] T. Qin, P. Li, and S. Shen. Vins-mono: A robust and versatile monocular visual-inertial state estimator. *IEEE Transactions on Robotics*, 34(4):1004–1020, 2018.
- [24] O. Ronneberger, P. Fischer, and T. Brox. U-net: Convolutional networks for biomedical image segmentation. In *International Conference on Medical image computing and computer-assisted intervention*, pages 234–241. Springer, 2015.
- [25] O. Russakovsky, J. Deng, H. Su, J. Krause, S. Satheesh, S. Ma, Z. Huang, A. Karpathy, A. Khosla, M. Bernstein, et al. Imagenet large scale visual recognition challenge. *International journal of computer vision*, 115(3):211–252, 2015.
- [26] A. Saxena, M. Sun, and A. Y. Ng. Make3d: Learning 3d scene structure from a single still image. *IEEE transactions on pattern analysis and machine intelligence*, 31(5):824–840, 2008.
- [27] J. L. Schonberger and J.-M. Frahm. Structure-from-motion revisited. In *Proceedings of the IEEE conference on computer vision and pattern recognition*, pages 4104–4113, 2016.
- [28] L. Tiwari, P. Ji, Q.-H. Tran, B. Zhuang, S. Anand, and M. Chandraker. Pseudo RGB-D for self-improving monocular SLAM and depth prediction. In *European Conference on Computer Vision*, pages 437–455. Springer, 2020.
- [29] Q. Zhou, T. Sattler, M. Pollefeys, and L. Leal-Taixe. To learn or not to learn: Visual localization from essential matrices. In *2020 IEEE International Conference on Robotics and Automation (ICRA)*, pages 3319–3326. IEEE, 2020.
- [30] T. Zhou, M. Brown, N. Snavely, and D. G. Lowe. Unsupervised learning of depth and ego-motion from video. In *Proceedings of the IEEE conference on computer vision and pattern recognition*, pages 1851–1858, 2017.